PAULING, L. (1977). *Proc. Natl Acad. Sci. USA*, **74**, 2614–2615.
PLASTAS, H. J., STEWART, J. M. & GRIM, S. O. (1973). *Inorg. Chem.* **12**, 265–272.
RANKIN, D. W. H. & ROBERTSON, A. (1976). *J. Organomet. Chem.* **105**, 331–340.
ROBIETTE, A. G., SHELDRICK, G. M., SIMPSON, R. N. F., AYLETT, B. J. & CAMPBELL, J. M. (1968). *J. Organomet. Chem.* **14**, 279–285.
ROBINSON, W. T. & IBERS, J. A. (1967). *Inorg. Chem.* **6**, 1208–1213.
ROBINSON, W. T. & SCHUSSLER, D. P. (1973). *Inorg. Chem.* **12**, 847–854.
SASSE, H. E. & ZIEGLER, M. L. (1972). *Z. Anorg. Allg. Chem.* **392**, 167–172.
SEIP, H. M. & SEIP, R. (1970). *Acta Chem. Scand.* **24**, 3431–3432.
SKAPSKI, A. C. & TROUGHTON, P. G. H. (1968). *Chem. Commun.* pp. 1230–1231.
SMITH, M. B. & BAU, R. (1973). *J. Am. Chem. Soc.* **95**, 2388–2389.
STALICK, J. K. & IBERS, J. A. (1969). *Inorg. Chem.* **8**, 419–423.
VAHRENKAMP, H. (1972). *Chem. Ber.* **105**, 1486–1496.
VAHRENKAMP, H. & NÖTH, H. (1973). *Chem. Ber.* **106**, 2227–2235.
WEBER, H. P. & BRYAN, R. F. (1967). *Acta Cryst.* **22**, 822–836.
WHITAKER, A. & JEFFERY, J. W. (1967). *Acta Cryst.* **23**, 977–984.

Acta Cryst. (1978). B**34**, 752–758

High-Temperature Phases of $SrZrO_3$

BY M. AHTEE

Department of Physics, University of Helsinki, Siltavuorenpenger 20 D, SF00170 Helsinki 17, Finland

A. M. GLAZER

Clarendon Laboratory, Parks Road, Oxford OX1 3PU, England

AND A. W. HEWAT

Institut Laue–Langevin, Grenoble, France

(*Received* 16 *August* 1977; *accepted* 30 *September* 1977)

The high-temperature structures of $SrZrO_3$ have been determined by neutron powder profile refinement, and the phase transitions described by the condensation of soft vibrational modes. At 900°C, $SrZrO_3$ is tetragonal, $I4/mcm$, with an O octahedron antiphase tilt of 6·5° about [001], intermediate between those found in the isomorphous phases of $SrTiO_3$ below 110 K and $KMnF_3$ below 184 K. At 760°C the structure is orthorhombic $Bmmb$ with almost equal b_o and c_o axes, and not tetragonal. In addition to the antiphase tilt, now 8·5° about [001], there is an in-phase tilt of 3·1° about [010]. Yet a third tilt, antiphase about [100] and identical to that about [001], is introduced at room temperature. This series of transitions indicates that the sequence of condensation of soft modes from the high-temperature cubic phase is R_{25}, M_3 and finally R_{25} again. In addition, the two latter transitions are first order, and are accompanied by a condensation from the X-point of the Brillouin zone, which produces atomic displacements. The unusually anisotropic thermal ellipsoids provide some additional evidence for the existence of low-frequency vibrational modes.

Introduction

Carlsson (1967) has studied the high-temperature phase transitions in $SrZrO_3$ by differential thermal analysis and X-ray diffraction. He found the following sequence of phase transitions:

orthorhombic $\xrightarrow{700\,^\circ C}$ tetragonal ($c/a < 1$) $\xrightarrow{830\,^\circ C}$ tetragonal ($c/a > 1$) $\xrightarrow{1170\,^\circ C}$ cubic.

In an earlier paper (Ahtee, Ahtee, Glazer & Hewat, 1977) the structure of $SrZrO_3$ at room temperature was reported, solved by the neutron powder profile refinement technique (Rietveld, 1969; Hewat, 1973). In this paper we report the structures of the two high-temperature phases at 760 and 900°C and also consider the possible soft modes associated with the corresponding transitions.

Data collection

Neutron diffraction measurements were made on the D1A high-resolution powder diffractometer on the high-

flux reactor at the ILL (Grenoble). D1A has been modified since the earlier measurements on $SrZrO_3$ at room temperature by the addition of a bank of ten ^3He high-pressure counters with 6° angular separation (Hewat & Bailey, 1976). The system is about 40 times as efficient as before. In the measurements described here, we used the intensities from seven counters merged together, with the counter bank sweeping through $2\theta = 0$ to 160° in steps of 0·05°. The wavelength was 1·387 Å.

Structure of $SrZrO_3$ at 900°C

In Fig. 1 the neutron powder pattern of $SrZrO_3$ at 900°C is shown, some of the reflections being indexed on the basis of the double pseudocubic perovskite subcell. In addition to the main reflections (all indices even) superlattice reflections with all indices odd are observed indicating antiphase (–) tilts of adjacent O octahedra. According to the classification of octahedral tilts (Glazer, 1972, 1976) this fact, together with the assumption of tetragonal symmetry, suggests the tilt system $a^0a^0c^-$ with space group $I4/mcm$; this structure is also found in $KMnF_3$ below 184 K (Minkiewicz, Fujii & Yamada, 1970) and $SrTiO_3$ below 110 K (Shirane & Yamada, 1969).

Instead of the pseudocubic orientation it is more usual to specify the tetragonal unit cell according to axes chosen by the matrix

$$\begin{array}{c} \\ a_o \\ b_o \\ c_o \end{array} \begin{array}{c} \begin{array}{ccc} a_p & b_p & c_p \end{array} \\ \begin{pmatrix} \frac{1}{2} & \frac{1}{2} & 0 \\ \frac{1}{2} & \frac{1}{2} & 0 \\ 0 & 0 & 1 \end{pmatrix} \end{array}$$

where a_o, b_o, c_o are the tetragonal axes with $a_o = b_o = \sqrt{2}a_p = \sqrt{2}b_p$ and $c_o = c_p$. In Fig. 2 this conventional tetragonal cell is drawn in relation to the pseudocubic cell. The tilting of the O octahedra is sketched in the figure (exaggerated for clarity). The atomic coordinates in the conventional tetragonal orientation are given in Table 1 in terms of the displacements u, v and w from the special positions of the ideal cubic perovskite structure.

Table 1. *Displacement u, v and w from the cubic perovskite positions in space group I4/mcm in the conventional tetragonal orientation and the corresponding symmetry restrictions on anisotropic temperature factor parameters (Peterse & Palm, 1966)*

		x	y	z	
Sr	4(*b*)	0	$\frac{1}{2}$	$\frac{1}{4}$	$B_{11} = B_{22} \neq B_{33}$
Zr	4(*c*)	0	0	0	$B_{11} = B_{22} \neq B_{33}$
O(1)	4(*a*)	0	0	$\frac{1}{4}$	$B_{11} = B_{22} \neq B_{33}$
O(2)	8(*h*)	$\frac{1}{4} + u$	$\frac{3}{4} + u$	0	$B_{11} = B_{22} \neq B_{33} \neq B_{12}$

The structural parameters, *i.e.* lattice parameters, fractional coordinates and both isotropic and anisotropic temperature factors, were refined with Rietveld's refinement program modified by A. W. Hewat (ILL Report 74/H625, April 1974). One effect found during the refinement was the considerably better agreement between the observed and calculated intensities of certain reflections when anisotropic temperature factors were included in the refinement (Table 2). The atomic positions and isotropic and anisotropic temperature factors are given in Table 3. It can be seen that the atomic positions do not depend severely on whether isotropic or anisotropic temperature factor refinement is carried out.

Fig. 3 shows the environment of the Zr and Sr cations from the data refined with anisotropic temperature factors. The ZrO_6 octahedron is very regular, the strain being only

$$\frac{\text{ZrO(1)–ZrO(2)}}{\langle \text{Zr–O} \rangle} \times 100 = 0{\cdot}4\%.$$

The angle of tilt of the octahedron about [001] is 6·5 (9)° which is considerably larger than that found in $SrTiO_3$ at 110 K [1·4 (4)° (Shirane & Yamada, 1969)]. On the other hand it is smaller than the 9·1° found in $KMnF_3$ at 145 K (Minkiewicz, Fujii & Yamada, 1970). The value for $SrZrO_3$ therefore seems reasonable.

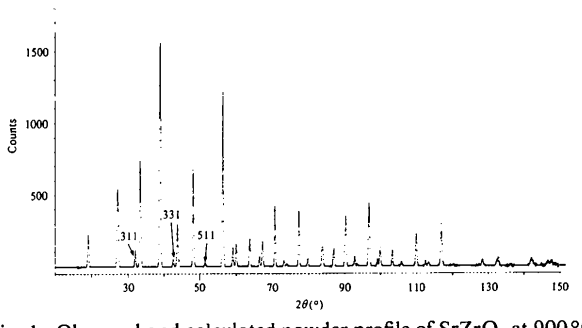

Fig. 1. Observed and calculated powder profile of $SrZrO_3$ at 900°C.

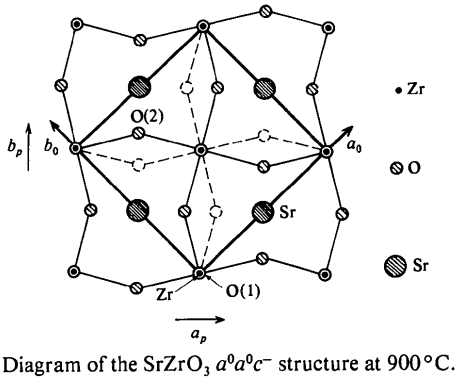

Fig. 2. Diagram of the $SrZrO_3$ $a^0a^0c^-$ structure at 900°C.

Table 2. *Comparison of the observed (I_o) and calculated intensities when either the isotropic [I_c(iso.)] or anisotropic [I_c(aniso.)] temperature factors were included in the refinement at* 900 °C

h k l	I_o	I_c(iso.)	I_c(aniso.)
2 0 4	5168	3970	5315
3 1 2			
1 1 6	1147	2340	1568
3 3 2			
4 2 0			
2 2 6	90	369	78
4 1 5	151	277	180
2 0 8	3300	1914	3022
3 3 6			
5 3 2			
6 0 0			
3 1 8	1208	608	967
5 3 4			
6 2 2			
6 1 5	188	318	252
6 3 3			
4 1 9	77	187	85
6 3 5			
7 2 3			
6 4 4	443	619	382
7 3 2			
6 1 7	28	130	51

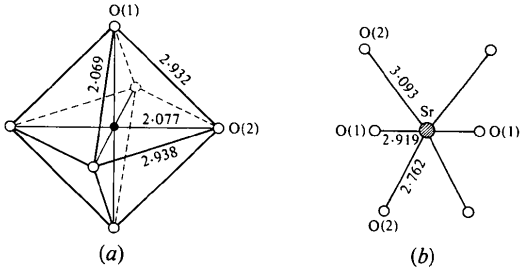

Fig. 3. Environment of the cations at 900 °C: (*a*) Zr, (*b*) Sr.

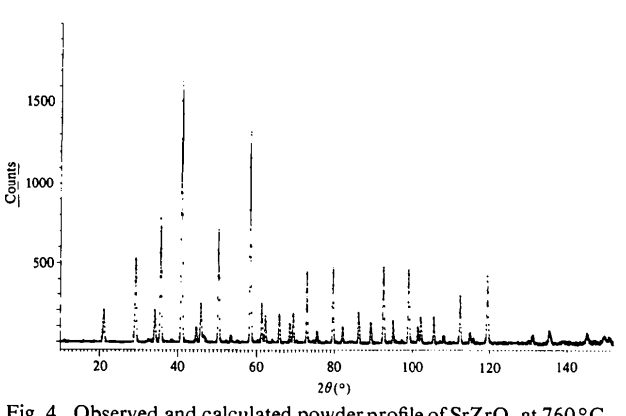

Fig. 4. Observed and calculated powder profile of $SrZrO_3$ at 760 °C. The small extra intensity at 47° is due to the furnace.

Table 3. *Structural parameters in tetragonal* $SrZrO_3$ *at* 900 °C

Isotropic temperature factor refinement

	B (Å^2)		B (Å^2)
Sr	3·14 (7)	O(1)	7·88 (41)
Zr	1·42 (5)	O(2)[u = 0·0274 (5)]	2·92 (7)

a_o = 5·8516 (3) Å c_o = 8·2956 (7) Å*

$R_{nuclear}$ = 14·54% $R_{profile}$ = 20·19% $R_{expected}$ = 5·73%

Anisotropic temperature factor refinement

Sr	B_{11} = 3·07 (8) Å^2	O(1)	B_{11} = 9·17 (37) Å^2
	B_{33} = 2·69 (14)		B_{33} = 0·67 (14)
Zr	B_{11} = 2·01 (7)	O(2)[u = 0·0278 (4)]	B_{11} = 2·65 (7)
	B_{33} = 0·37 (9)		B_{33} = 6·03 (20)
			B_{12} = 1·39 (12)

a_o = 5·8504 (2) Å c_o = 8·2952 (3) Å*

$R_{nuclear}$ = 7·34% $R_{profile}$ = 13·18% $R_{expected}$ = 5·72%

* Standard errors in the lattice parameters do not include error in neutron wavelength.

Structure of $SrZrO_3$ at 760 °C

The diffraction pattern in Fig. 4 shows that in addition to the main perovskite reflections there are now some which when indexed on the doubled pseudocubic subcell have all odd indices and some with two odd and one even. The former type of reflection suggests anti-phase tilts (−) of octahedra and the latter in-phase tilts (+). According to Glazer's classification it is impossible to construct a tetragonal crystal with both + and − tilts and therefore this phase cannot be tetragonal as described by Carlsson (1967). The most likely explanation is that the phase is orthorhombic with two axes very similar in length. This leads us to suggest the tilt system $a^0b^+c^-$ with space group *Bmmb*. Table 4 lists the displacement coordinates with respect to the ideal cubic perovskite positions. In this space group the Sr atoms can be displaced along [001] in antiparallel layers perpendicular to [010]. The two independent Sr atoms within a layer are assumed to be displaced in the same sense; this is suggested by considering the approach of the O atoms under the proposed tilting arrangement, the Sr atom positions being dictated by the need to equalize all Sr–O distances. The displacements give rise to reflections with one odd index. These are very weak in Fig. 4, presumably because the Sr displacements are small. Two layers perpendicular to [010] are shown in Fig. 5.

Refinement of this model was carried out and the results are listed in Table 5. As in the tetragonal phase, the positional parameters are hardly affected by

whether the refinement includes isotropic or anisotropic temperature factors. Sr(1) is displaced along **c** by about 0·08 Å whereas Sr(2) is undisplaced within the error limits. This is easy to understand by examining the environment of the Sr atoms in Fig. 5. For Sr(1) there are two nearest-neighbour O(2) atoms, which tend to push the Sr atom along [00$\bar{1}$] in the first layer and along [001] in the second. On the other hand, Sr(2) is held central by its nearest neighbours which form an approximate square about it. The next-nearest neighbours are two O(3) atoms which may provide a very slight push of Sr(2) along [00$\bar{1}$] on the first layer and along [001] on the second. The tilt around [001] displaces O(2) along [010] and O(3) along [100]. These displacements are equal giving a tilt angle of 8·5 (3)°. Tilting around [010] displaces O(1) along [100] and O(2) along [001] but in this case there is a small distortion of the O octahedron ($u_1 \neq w_2$) giving the average value of the tilt angle as 3·1 (6)°.

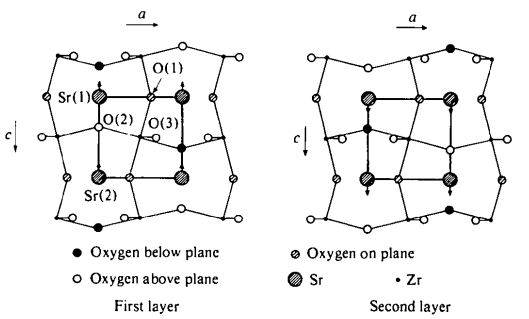

Fig. 5. Diagram of the $SrZrO_3$ $a^0b^+c^-$ structure at 760°C.

It is interesting to compare the tilt angles here with those in the room-temperature phase (Ahtee, Ahtee, Glazer & Hewat, 1977). The change in structure on lowering the temperature to below 700°C can be understood with reference to Fig. 5. In this phase, the Sr atoms on the first layer are displaced along [10$\bar{1}$]

Table 4. *Displacements u, v, w from the cubic perovskite positions in space group Bmmb and the corresponding symmetry restrictions on the anisotropic temperature factor parameters*

		u	v	w	
Sr(1)	4(*c*)	0	$\frac{1}{4}$	w_{A1}	$B_{11} \neq B_{22} \neq B_{33}$
Sr(2)	4(*c*)	0	$\frac{1}{4}$	$\frac{1}{2} + w_{A2}$	$B_{11} \neq B_{22} \neq B_{33}$
Zr	8(*d*)	$\frac{1}{4}$	0	$\frac{1}{4}$	$B_{11} \neq B_{22} \neq B_{33} \neq B_{12} \neq B_{13} \neq B_{23}$
O(1)	8(*e*)	$\frac{1}{4} + u_1$	0	0	$B_{11} \neq B_{22} \neq B_{33} \neq B_{23}$
O(2)	8(*f*)	0	v_2	$\frac{1}{4} + w_2$	$B_{11} \neq B_{22} \neq B_{33} \neq B_{23}$
O(3)	8(*g*)	$\frac{1}{4} + u_3$	$\frac{1}{4}$	$\frac{1}{4} + w_3$	$B_{11} \neq B_{22} \neq B_{33} \neq B_{13}$

Table 5. *Structural parameters in orthorhombic* $SrZrO_3$ *at* 760°C

Isotropic temperature factor refinement

		B (Å²)			B (Å²)
Sr(1)	[$w_{A1} = -0.0064$ (21)]	2·64 (23)	O(2)	[$v_2 = 0.0449$ (11)]	2·36 (15)
Sr(2)	[$w_{A2} = -0.0011$ (21)]	2·57 (24)		[$w_2 = -0.0184$ (15)]	
Zr		1·05 (3)	O(3)	[$u_3 = 0.0332$ (9)]	1·86 (10)
O(1)	[$u_1 = 0.0135$ (16)]	4·08 (16)		[$w_3 = 0.0056$ (15)]	

$a_o = 8.2353$ (4) Å $b_o = 8.2500$ (7) Å $c_o = 8.2522$ (6) Å
$R_{nuclear} = 12.85\%$ $R_{profile} = 19.45\%$ $R_{expected} = 12.85\%$

Anisotropic temperature factor refinement

Sr(1)	[$w_{A1} = -0.0107$ (17)]	$B_{11} = 2.52$ (36) Å²	O(1)	[$u_1 = 0.0114$ (18)]	$B_{11} = 5.01$ (46) Å²
		$B_{22} = 2.79$ (71)			$B_{22} = 6.44$ (72)
		$B_{33} = 1.49$ (40)			$B_{33} = 0.87$ (19)
Sr(2)	[$w_{A2} = -0.0033$ (18)]	$B_{11} = 2.18$ (40)			$B_{23} = -0.76$ (37)
		$B_{22} = 2.82$ (63)	O(2)	[$v_2 = 0.0349$ (12)]	$B_{11} = 0.58$ (16)
		$B_{33} = 2.73$ (48)		[$w_2 = -0.0137$ (16)]	$B_{22} = 1.94$ (33)
Zr		$B_{11} = 1.22$ (17)			$B_{33} = 6.75$ (60)
		$B_{22} = 1.96$ (31)			$B_{23} = 0.74$ (34)
		$B_{33} = 0.10$ (15)	O(3)	[$u_3 = 0.0399$ (14)]	$B_{11} = 2.84$ (25)
		$B_{12} = -0.04$ (22)		[$w_3 = 0.0059$ (14)]	$B_{22} = 1.08$ (23)
		$B_{13} = 0.24$ (26)			$B_{33} = 3.65$ (82)
		$B_{23} = 0.14$ (17)			$B_{13} = 0.22$ (44)

$a_o = 8.2532$ (3) Å $b_o = 8.2662$ (5) Å $c_o = 8.2709$ (4) Å
$R_{nuclear} = 6.74\%$ $R_{profile} = 14.35\%$ $R_{expected} = 6.74\%$

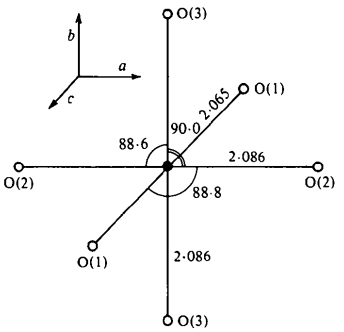

Fig. 6. Bond lengths (Å) and angles (°) in the ZrO_6 octahedron at 760°C.

while those on the second are along [101]. In addition, O(1) is displaced below the plane with the other O atoms also displaced in such a way as to give the $a^-b^+a^-$ tilt system. [This is shown in Fig. 2(*a*) of the paper on the room-temperature structure, but there the axes were labelled differently to give the $a^-a^-c^+$ tilt system.] The tilt angle about [001] is 8°, which is close to that in the 760°C phase. However, there is now a second tilt of the same magnitude about [100] (there are two antiphase tilts). The in-phase tilt about [010] is 7·6° in the room-temperature phase, a value which is a little over twice that in the 760°C phase.

In Fig. 6 the bond lengths and angles of the ZrO_6 octahedron at 760°C are given. The major bond-length distortion is a compression of about 1% along [001], the same direction as the Sr displacements. This coincides also with the small value of B_{33} for the Zr atom.

Soft modes

It has been shown that the phase transitions in some perovskites, *e.g.* $SrTiO_3$, $KMnF_3$, $NaNbO_3$, $LaAlO_3$, are caused by the condensation of a soft normal mode of vibration associated with the rotations of the octahedra in the cubic phase, and that the eigenvectors of this mode are the same as the static displacements of the atoms in the lower-symmetry phases (*e.g.* Glazer & Megaw, 1972; Ahtee, Glazer & Megaw, 1972; Fujii, Hoshino, Yamada & Shirane, 1974). The static displacements in $SrTiO_3$ and $KMnF_3$ ($a^0a^0c^-$) can be attributed to the condensation of a single component of the triply-degenerate R_{25} mode* in which the adjacent octahedra (Fig. 7) along an axis vibrate about the axis in opposite senses. In $NaNbO_3$ the displacements in the high-temperature T_2 phase ($a^0a^0c^+$) arise out of condensation of the M_3 mode (Fig. 7) in which the adjacent octahedra vibrate in the same sense.

It is possible to use this soft-mode picture to explain the sequence of phases in $SrZrO_3$. Here the sequence of tilting is represented by

$$a^-b^+a^- \underset{700\,^\circ C}{\rightleftarrows} a^0b^+c^- \underset{830\,^\circ C}{\rightleftarrows} a^0a^0c^- \underset{1170\,^\circ C}{\rightleftarrows} a^0a^0a^0.$$

The obvious soft-mode condensation on cooling from the cubic phase is $R_{25} \rightarrow M_3 \rightarrow R_{25}$. We should, however, recognize that the 700 and 830°C transitions are of first order. In simple soft-mode terms we expect condensation of at least one other mode at each transition. This will probably be that mode which gives rise to the cation displacement configuration. For example, in order to explain the displacements of Sr(1) and O(3) along [001] in the 760°C phase of $SrZrO_3$ we can assume condensation of a doubly-degenerate mode at the X-point of the Brillouin zone (Darlington, 1976). This type of condensation occurs in phases III and IV of $CsPbCl_3$ (Fujii *et al.*, 1974) and in $CsPbBr_3$ (Hirotsu, Harada, Iizumi & Gesi, 1974). The symmetry-adapted vectors for one component of this mode are shown in Fig. 8 and thus condensation of one component gives the displacements in the 760°C phase. The phase below will then be found by a further condensation at the X-point.

It is tempting to see if there is any evidence for such soft-mode behaviour from our structural results. The thermal ellipsoids are an average over all normal modes. However, when a soft mode exists in the crystal, it is possible that its amplitude will so dominate the temperature factor as to produce an unusually anisotropic thermal ellipsoid (Hewat, 1972; Abrahams & Bernstein, 1974).

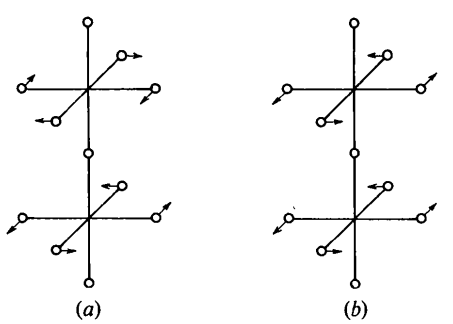

Fig. 7. Symmetry-adapted vectors for (*a*) the R_{25} and (*b*) the M_3 modes.

* We shall use the group-theoretical symbols for representations pertaining to the cubic phase, even though the phase we consider may not be cubic, but pseudocubic.

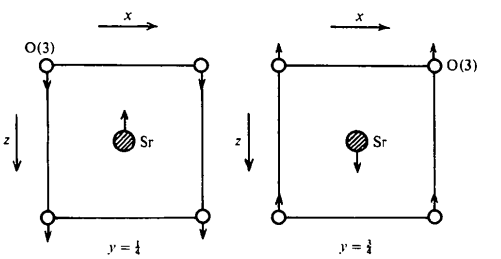

Fig. 8. Symmetry-adapted vectors for a component of the X mode.

Often neutron powder techniques are unreliable for temperature-factor measurements, largely because of the relatively low-angle cut-off in the data. However, our high-resolution data (Fig. 1) extend to $\sin\theta/\lambda = 0{\cdot}71$ Å^{-1}, beyond the limit for Cu $K\alpha$ X-radiation. In addition, experience with powder refinements on other materials such as $K(Ta,Nb)O_3$ (Hewat, 1972, 1973; Abrahams & Bernstein, 1974) and $NH_4H_2PO_4$ (Hewat, 1977), does seem to show a consistency in the orientation of the thermal ellipsoids; if they are very anisotropic they probably indicate a soft vibrational mode which may condense to produce a phase transition at lower temperatures. We shall therefore attempt to understand our temperature factors in terms of the soft-mode picture postulated above, especially where the ellipsoids are very anisotropic.

Consider first the tetragonal phase. From Table 3 it is clear that there is a strong anisotropy in the thermal ellipsoids for O(1) and O(2). For both atoms the amplitude of vibration is smallest along the Zr–O bonds in accordance with a rigid-body rotation of the octahedron. Fig. 9 shows schematically the directions of the largest vibrational amplitudes in the O octahedron and how they are decomposed into two equal oscillations A and B about pseudocubic [100] and [010]. Since throughout the phase transitions both M_3 and R_{25} modes must condense to give + and − tilts, it is fair to assume that all modes from the R to the M point are soft, as is seen in $NaNbO_3$ and $KMnF_3$, for example. The motion illustrated in Fig. 9 can be interpreted as the sum over the R_{25}–M_3 modes whose symmetry-adapted vector components are about pseudocubic [100] and [010]. The component about [001] is small since an R_{25} mode has condensed to form the c^- tilt of the 900 °C structure. Part of the vibration about [010] in Fig. 9 would be the M_3 mode that condenses to give the b^+ tilt of the 760 °C phase.

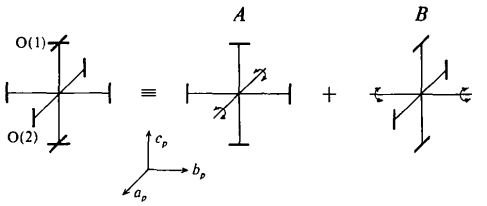

Fig. 9. Schematic diagram of the largest vibrational amplitudes of the atoms and their decomposition into two components.

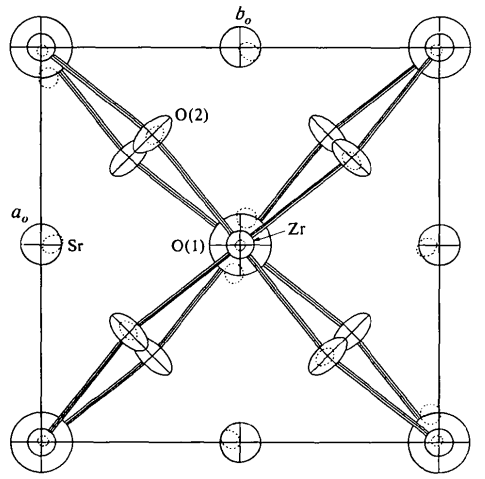

Fig. 10. *ORTEP* plot of the 900 °C phase, showing how the thermal ellipsoids just contain the atomic positions in the room-temperature phase. (Dotted lines indicate the thermal ellipsoids for the room-temperature phase.) Note that the extreme anisotropy of the O ellipsoids at 900 °C is consistent with a rigid oscillation of the O octahedron around [001].

Fig. 10 shows an *ORTEP* plot of this 900 °C phase on (001) with the thermal ellipsoids drawn to show the 50% probability limits of displacement. These thermal ellipsoids just contain the displaced atomic positions of the room-temperature phase (dotted). This is precisely what would be expected if this thermal motion were largely due to soft modes which condense to produce the room-temperature structure.

In the orthorhombic phase at 760 °C, it can be seen from Table 5 that the directions of smallest thermal amplitude for the O atoms are again along the Zr–O bonds. In fact, if it is assumed that B_{11} and B_{22} for O(1) are equal, which is true within experimental error, the motion looks the same as in the tetragonal phase. Therefore, Fig. 9 can be used equally for this phase. Vibration A is consistent with the soft-mode motion necessary to produce the a^- tilt in the next lowest phase. Vibration B on the other hand is motion about [010] which ought to be small since it is about this axis that a mode has already condensed to form the b^+ tilt. It could be that this represents the amplitude of the [010] component of the uncondensed R_{25} mode in this phase.

Thus it is seen that the thermal amplitudes derived here are consistent with a rigid-body vibration of the O octahedron and may well be indicative of soft-mode behaviour.

One of us (MA) acknowledges a grant from the Finnish Academy which made the visit to the ILL possible. AMG thanks the Wolfson Foundation and the Science Research Council for financial support. We thank the ILL for facilities.

References

ABRAHAMS, S. C. & BERNSTEIN, J. L. (1974). *Ferroelectrics*, **6**, 247–250.

AHTEE, A., AHTEE, M., GLAZER, A. M. & HEWAT, A. W. (1977). *Acta Cryst.* B**32**, 3243–3246.

AHTEE, M., GLAZER, A. M. & MEGAW, H. D. (1972). *Philos. Mag.* **26**, 995–1014.

CARLSSON, L. (1967). *Acta Cryst.* **23**, 901–905.

DARLINGTON, C. N. W. (1976). *Phys. Status Solidi B*, **76**, 231–239.

FUJII, Y., HOSHINO, S., YAMADA, Y. & SHIRANE, G. (1974). *Phys. Rev. B*, **9**, 4549–4559.

GLAZER, A. M. (1972). *Acta Cryst.* B**28**, 3384–3392.

GLAZER, A. M. (1976). *Acta Cryst.* A**31**, 756–762.
GLAZER, A. M. & MEGAW, H. D. (1972). *Philos. Mag.* **25**, 1119–1135.
HEWAT, A. W. (1972). *Phys. Status Solidi*, **53**, k33–k34.
HEWAT, A. W. (1973). *J. Phys. C*, **6**, 2559–2572.
HEWAT, A. W. (1977). Proc. Fourth Eur. Crystallogr. Meet., Oxford.
HEWAT, A. W. & BAILEY, I. (1976). *Nucl. Instrum. Methods*, **137**, 463–471.
HIROTSU, S., HARADA, J., IIZUMI, M. & GESI, K. (1974). *J. Phys. Soc. Jpn*, **37**, 1393–1398.
MINKIEWICZ, V. J., FUJII, Y. & YAMADA, Y. (1970). *J. Phys. Soc. Jpn*, **28**, 443–450.
PETERSE, W. J. A. M. & PALM, J. H. (1966). *Acta Cryst.* **20**, 147–150.
RIETVELD, H. M. (1969). *J. Appl. Cryst.* **2**, 65–71.
SHIRANE, G. & YAMADA, Y. (1969). *Phys. Rev.* **177**, 858–863.

Acta Cryst. (1978). B**34**, 758–762

The Crystal Structure of $La_7(OH)_{18}I_3$*

BY EDWARD THEODORE LANCE-GÓMEZ†

Chemistry Division, Argonne National Laboratory, Argonne, Illinois 60439, *USA*

JOHN M. HASCHKE

Rockwell International, Rocky Flats Plant, PO Box 464, *Golden, Colorado* 80401, *USA*

WILLIAM BUTLER

Department of Chemistry, University of Michigan, Ann Arbor, Michigan 48109, *USA*

AND DONALD R. PEACOR

Department of Geology and Mineralogy, University of Michigan, Ann Arbor, Michigan 48109, *USA*

(*Received* 22 *July* 1977; *accepted* 17 *October* 1977)

The crystal structure of hexagonal $La_7(OH)_{18}I_3$ (space group $P6_3/m$, $a = 18{\cdot}315 \pm 0{\cdot}007$, $c = 3{\cdot}928 \pm 0{\cdot}001$ Å, $Z = 2$) has been refined from diffractometer-collected intensity data by full-matrix least-squares methods to a conventional R of 2·9%. The structure is derived from that of the UCl_3-type trihydroxide by iodide substitution on one-seventh of the anion sites. The unit cell is a complex arrangement of two regular and six slightly irregular trigonal prisms of $La(OH)_3$ plus six highly distorted trigonal prisms of $La(OH)_2I$ produced by accommodation of iodide ions in vacant channels of the parent structure. This type of accommodation mechanism maintains ninefold cation coordination and accounts for the occurrence of this structure type for several monovalent anions with substantially different sizes. The space groups of the substructure and superstructure have a single same-class subgroup relationship. The superstructure is the first example of the previously unknown $m = 7$ member of the {3,6} compound-tessellation series.

Introduction

Recent investigations (Haschke & Eyring, 1971; Haschke, 1974; Lance & Haschke, 1976) of ternary lanthanide monovalent anion systems have succeeded in elucidating the structural relationships and crystal chemistry of lanthanide hydroxide halides and hydroxide nitrates. Qualitative comparisons and subgroup–supergroup correlations (Neubüser & Wondratschek, 1966; Wondratschek, 1974) have been used (Haschke, 1976, 1977) to demonstrate the existence of close relationships between the structures. The $Y(OH)_2Cl$-type structure of the $Ln(OH)_2X$ phases (Ln = lanthanide, $X = NO_3^-$, Cl^-) and the high-temperature form of $La(OH)_2NO_3$ are closely related to the UCl_3-type structures of the lanthanide trihydroxides and trihalides, and the $PuBr_3$-type structure of the lanthanide trihalides respectively. However, an adequate understanding of the crystal chemistry of the hydroxide halide and hydroxide nitrate phases of the lighter lanthanides is incomplete without structural knowledge of the phase which forms between the trihydroxide and the $Ln(OH)_2X$ phase.

* Abstracted in part from the PhD Dissertation of E. T. Lance-Gómez, University of Michigan.

† To whom correspondence should be addressed.